Master-oscillator power-amplifier quantum cascade laser array

Cite as: Appl. Phys. Lett. **101**, 261117 (2012); https://doi.org/10.1063/1.4773377
Submitted: 10 October 2012 . Accepted: 10 December 2012 . Published Online: 28 December 2012

P. Rauter, S. Menzel, A. K. Goyal, B. Gökden, C. A. Wang, A. Sanchez, G. W. Turner, and F. Capasso

Master-oscillator power-amplifier quantum cascade laser array

P. Rauter,[1] S. Menzel,[1] A. K. Goyal,[2] B. Gökden,[1] C. A. Wang,[2] A. Sanchez,[2] G. W. Turner,[2] and F. Capasso[1]
[1]*School of Engineering and Applied Sciences, Harvard University, 29 Oxford St., Cambridge, Massachusetts 02138, USA*
[2]*MIT Lincoln Laboratory, 244 Wood St., Lexington, Massachusetts 02420, USA*

(Received 10 October 2012; accepted 10 December 2012; published online 28 December 2012)

We report on the demonstration of an array of master-oscillator power-amplifier quantum cascade lasers (QCLs) operating in single-mode at different wavelengths between 9.2 and 9.8 μm. In each device, the output of a distributed feedback QCL is injected into a tapered QCL section which acts as an amplifier while maintaining a high beam quality due to adiabatic mode spreading. All array elements feature longitudinal as well as transverse single-mode emission at peak powers between 0.8 and 3.9 W at room temperature. The high output power and excellent beam quality render the array highly suitable for stand-off spectroscopy applications. © *2012 American Institute of Physics*. [http://dx.doi.org/10.1063/1.4773377]

Recently, the use of quantum cascade lasers (QCLs, Refs. 1 and 2) for stand-off detection[3,4] and spectroscopy[5] in the mid-infrared has increased the demand for wavelength-tunable sources of high output power and good beam quality. Up to now, such systems have employed external cavity QCLs,[6] where wavelength selection and continuous tuning require the rotation and translation of a grating. Arrays of single-mode QCLs are an alternative approach for a multi-wavelength QCL source.[7,8] Even though the performance of distributed feedback (DFB) QCLs is being steadily improved and continuous wave operation with 2.4 W output power has recently been demonstrated,[9] single-mode DFB QCLs as elements of an array have so far been limited in their peak output power. An increase of the volume of the gain medium by increasing the laser ridge width above a certain value results in higher-order lateral modes which compromise beam quality. The integration of a quantum cascade optical amplifier[10] with a DFB QCL has demonstrated the possibility to combine the excellent beam quality of a DFB QCL with high power amplification in a monolithically integrated device.[11] The monolithically integrated master-oscillator power-amplifier (MOPA) configuration had been applied to diode lasers[12,13] for considerable time until its realization based on a QCL.[11] Only very recently high-power, single-mode operation of a QCL MOPA reaching peak powers of 1.5 W has been reported.[14] QCL MOPAs are two-section devices composed of a low-power single-mode DFB seed laser and a tapered power amplifier. The output of the DFB section is coupled into the amplifier, which is current driven below its self-lasing threshold. The excellent beam quality of the DFB laser is preserved throughout the amplifier due to adiabatic mode expansion: The gradual increase in the amplifier cross section allows the spreading of the mode over a larger volume, thus, overcoming the intrinsic problem of gain saturation and reducing the lateral beam divergence. In this work, we report on the demonstration of an array of single-mode high-power MOPA QCLs operating at different wavelengths between 9.2 and 9.8 μm with room-temperature peak powers of up to 3.9 W and an overall excellent beam quality.

The material used for our MOPA array is an InGaAs/AlInAs broadband bound-to-continuum heterostructure[15] grown on a conducting InP substrate by organometallic vapor-phase epitaxy (OMVPE). A 3.5 μm thick, highly doped InP layer ($n = 1 \times 10^{17}$cm^{-3}) is followed by a 0.52 μm thick InGaAs layer ($n = 3 \times 10^{16}$cm^{-3}), and the active region. The latter is composed of 35 periods of the following layer sequence (InAlAs barriers bold, InGaAs wells roman, thickness in nm, underlined layers doped to $n = 1.5 \times 10^{17}$cm^{-3}): **4.4**/1.7/**0.9**/5.3/**1.1**/5.2/**1.2**/4.7/**1.3**/4.2/**1.5**/3.9/**1.6**/3.4/**1.8**/3.1/**2.1**/2.8/**2.5**/2.7/**3.2**/2.7/**3.6**/2.5. Following the growth of an additional injector sequence and 520 nm of GaInAs ($n = 3 \times 10^{16}$cm^{-3}), the structure is completed by the upper waveguide cladding formed by 3.5 μm of InP ($n = 1 \times 10^{17}$cm^{-3}) and the top contact layer composed of 0.5 μm of InP ($n = 5 \times 10^{18}$ cm^{-3}) and 20 nm of InGaAs ($n = 1.8 \times 10^{19}$cm^{-3}).

The sixteen MOPA QCL devices of the array comprise a DFB section sufficiently narrow for transverse single-mode operation, and a tapered amplifier section. In order to allow the fabrication of DFB gratings, the top InP cladding layer was removed by wet etching in a HCl : H_2O (1:1) solution. A first-order Bragg grating, including a central quarter-wave-shifted (QWS) region, was defined for the individual DFB lasers by electron-beam lithography and subsequent ion-etching into the now exposed 500 nm thick InGaAs layer with an etch-depth of 250 nm. To allow a different emission wavelength for each array element, the grating period was increased from device to device between 1.44 μm (device 1) and 1.55 μm (device 16).

The choice of a QWS DFB grating for the MOPA seed sections is based on the following consideration. As commonly known, the precise selection of a single mode in DFB lasers is difficult due to the influence of the reflectivity of the end facets (see, e.g., Ref. 8). Both modes at the edge of the photonic bandgap can experience comparable losses depending on the position of the end facets relative to the grating. The relative phase of the two modes with respect to the facets can lead to a variability and uncertainty in which mode can lase. In case of a multi-wavelength array of DFB devices, this is of particular concern as *all* of the ridge facets are

defined by a *single* cleave along a crystal plane. Due to the difference in the grating period from device to device, the facet reflection influences each device *differently*. According to Ref. 8, an anti-reflection (AR) coating on both facets of a QCL can eliminate this uncertainty in the selection of the lasing wavelength. In addition to AR coatings, the introduction of a QWS into the DFB grating has been employed for diode lasers.[16] The QWS pins the lasing wavelength to the spectral position of the low-threshold defect state generated in the center of the photonic bandgap and thus ensures reliable lasing at the design wavelength, where an AR coating on both facets is required in order to guarantee single-mode operation.[16]

Following the etching of the DFB grating, the InP cladding and top-contact layer were regrown using OMVPE. The MOPA ridges were defined by reactive ion-etching of double trenches. Careful design of the ridge geometry was crucial to ensure single-mode operation. The MOPA concept is based on seeding a spectrally clean single TM_{00} mode by driving a low-power DFB section. To suppress lasing on higher order lateral modes in the latter, sufficiently narrow DFB ridges of 13 μm width were implemented. A small tapering angle of 1.3 ° was chosen, which according to finite-difference time-domain calculations ensures adiabatic spreading of the seeded DFB mode in the amplifier. Following the deposition of 450 nm thick SiN, a Ti/Au metallization was applied as a ridge top contact. For proper amplifier operation, the tapered section has to be driven below the self-lasing threshold. The simultaneous driving of the DFB section close to peak power (rollover) is made possible by electrically separating both sections by a 100 μm wide gap in the gold metallization. The lengths of the individual DFB and power-amplifier sections (2 mm each) were defined by two cleaving steps, resulting in a 110 μm wide output facet of the MOPA devices. As discussed above, it is essential for reliable single-mode operation of the DFB sections to suppress the influence of the back facet mirror on the mode selection.[8] This is achieved by leaving 360 μm of the 2 mm long seed section unpumped (absorber segment in Fig. 1). Figure 1 shows a top view photograph of three array elements before packaging.

In order to increase the self-lasing threshold of the amplifier section, an AR coating was applied to the front facet of the array elements, allowing for strong optical amplification in single-pass travelling-wave configuration at high amplifier currents while conserving the beam and spectral quality of the seed mode. The AR coating is composed of a 842 nm thick layer of ZnS (refractive index of 2.2), and 1280 nm of YF_3 (refractive index 1.415), where adhesion between the layers is provided by 30 nm of Y_2O_3.

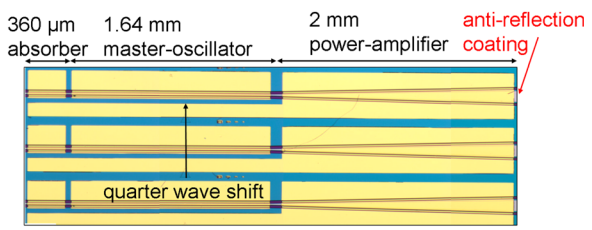

FIG. 1. Top view of three elements of the MOPA array.

Each device of the MOPA array has been thoroughly characterized under pulsed operation (10 kHz repetition rate, 25 ns MO pulse length, 100 ns PA pulse length) at a heat sink temperature of 18 °C. The difference in the current pulse lengths between the DFB section and the amplifier is due to limitations of the two employed pulse generators. However, the length of the output radiation bursts is determined by the MO pulse length, as the amplifier is driven below self-lasing threshold, giving a duty cycle of 0.025%. Out of the 16 fabricated array elements, one was not lasing due to an electrical defect (device 14). While measuring the output spectra of the individual devices using a Fourier transform infrared spectrometer, both the current through the DFB and the amplifier section were optimized in order to achieve maximum output power, while maintaining spectral single-mode operation of the MOPA with a targeted side-mode suppression ratio (SMRS) of at least 20 dB. Figure 2 shows these spectra at maximum single-mode power for all of the devices along with the respective peak power measured using a calibrated bolometer. The plotted spectra in Fig. 2 show that each array element operates at a different wavelength between 9.15 μm (device 1) and 9.77 μm (device 16), demonstrating the realization of a multi-wavelength MOPA array based on varying the DFB gratings of the individual seed sections. All of the devices are capable of single-mode operation at peak powers in excess of 0.8 W, with eleven MOPAs featuring single-mode peak powers at or above 1.5 W, which has been the highest value for single-mode operation of a QCL MOPA up to now.[14] Eight array elements feature single-mode peak powers of at least 2 W, with one device reaching 3.9 W. These high peak output powers are reached while showing a good SMSR as seen from a logarithmic plot of a selection of the spectra in Fig. 3. The corresponding values for the SMSR are listed on the right of the respective spectra in Fig. 2. Note that for two devices a SMSR of 20 dB could not be reached due to lasing at multiple modes even at low driving currents (devices 7 and 10 with 15 and 18 dB, respectively). However, 13 out of 15 array elements exhibit a SMSR of at least 20 dB for the peak power values given in Fig. 2.

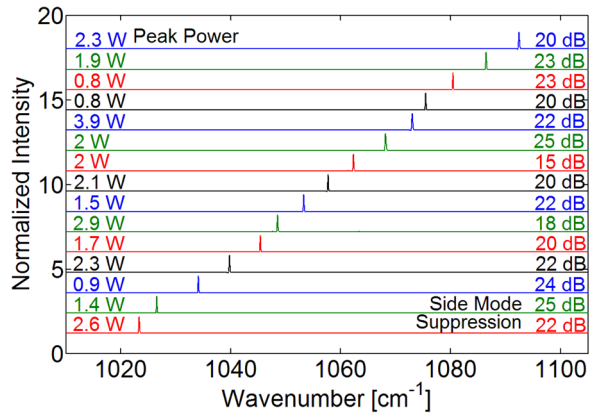

FIG. 2. Emission spectrum of MOPA array. For each device of the array, the spectrum at maximum single-mode peak power is shown together with the respective power values (on the left) and side-mode suppression ratio (values on the right). The spectra have been normalized to their maximum and offset vertically for clarity. The top and bottom curves represent device 1 and device 16, respectively, excluding the defective device 14. All measurements were performed at room temperature and a duty cycle of 0.025%.

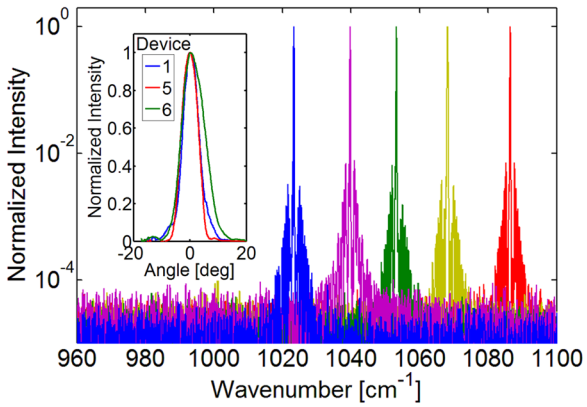

FIG. 3. Side-mode suppression and far-field. The logarithmic plots of a selection of the spectra in Fig. 2 demonstrate the good side-mode suppression ratio of the MOPA devices. The inset shows the excellent angular in-plane distribution of the far-field intensity for a selection of representative devices measured under conditions for maximum single-mode power. Nine devices show diffraction-limited TM_{00}-operation like device 5 (red curve). Five devices exhibit minor contributions of higher order lateral modes, while still maintaining an excellent far-field quality, as represented by the blue curve showing data on device 1.

The reason for the differing maximum single-mode peak-power values of the array elements can be attributed to a persistent influence of the device facets on the operation of the DFB seed sections. The inset of Fig. 4 shows the individual DFB and amplifier currents, at which the spectra for maximum single-mode power presented in Fig. 2 were obtained. The array elements can be divided into two groups: The devices which exhibit single-mode operation for DFB currents close to rollover (devices 1, 5, 6, 7, 8, 10, and 16), and those which show multi-mode behavior at high currents close to rollover and have to be driven at lower currents for single-mode operation (devices 2, 3, 4, 9, 11, 12, 13, and 15). As evident from light/DFB-current characteristics at fixed amplifier current (not shown), all of the array elements except device 3 exhibit a DFB rollover around 2 A, which is marked by the red horizontal line in the inset of Fig. 4. The DFB section of device 3 suffers from current leakage and reaches its rollover at 3 A. All of the devices capable of single-mode operation close to rollover feature single-mode peak powers of at least 2 W (also marked by the red horizontal line in Fig. 4). Device 5 reaches the highest value of 3.9 W as it can be driven simultaneously at the highest DFB current and amplifier current among these devices. The DFB sections of these seven devices thus can be driven under optimal conditions, allowing to seed a single mode at the maximum power possible, before the output intensity drops due to a misalignment of the electronic levels in the active region.

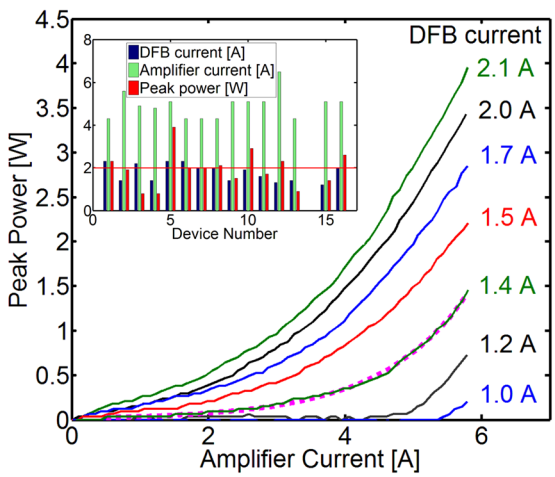

FIG. 4. Light/amplifier-current characteristics. The curves show the peak output power of device 5 as a function of the amplifier current for a series of DFB currents. Note the exponential growth of the peak power with amplifier current for a DFB current of 1.4 A, which is characteristic for amplifier operation in contrast to the linear increase expected for self-lasing. The pink, dotted line represents an exponential fit, allowing the extraction of the modal gain coefficient of the amplifier. For higher DFB currents, gain saturation sets in, leading to a deviation from the exponential behavior. The inset presents the values for DFB (blue bars) and amplifier current (green bars) for maximum single-mode power (red bars) for each array element. The spectra corresponding to these values are shown in Fig. 2.

On the other hand, even though devices 2, 3, 4, 9, 11, 12, 13, and 15 feature good single-mode operation at peak output powers of at least 0.8 W, their full seeding potential cannot be exploited due to multi-mode operation at higher DFB currents. As indicated by light/DFB-current characteristics (not shown), only about half of the maximum seeding power deliverable by the DFB sections of these devices is available for single-mode operation. An increase in the DFB current beyond the values presented in the inset of Fig. 4, which are far below rollover, leads to the appearance of additional modes. This is a strong indication for a residual influence of the back facet mirror on the lasing mode of the DFB section. As a consequence, the maximum single-mode output power of these devices lies below 2 W (red horizontal line in Fig. 4), with device 12 being the only exception. Device 12 reaches peak powers of 2.3 W at an exceptionally high amplifier current of 6.5 A in comparison to the other array elements, and at a very low DFB current of 1.3 A. Therefore, the high-power operation of device 12 at these extreme parameters is most likely based on self-lasing of the amplifier section, where the DFB section acts as a distributed Bragg reflector and selects the single mode of operation.

To summarize, seven of the fifteen array elements could be driven under ideal pumping conditions which utilize the maximum output power of the DFB section for single-mode operation. While the remaining eight devices still show single-mode operation at competitive output powers of at least 0.8 W, their DFB sections do not live up to their full seeding capability. By improving the reliability of the array's DFB sections with respect to single-mode operation, all of the MOPA devices can be pushed to excellent power performance in future arrays.

In addition to high peak power values and spectral purity, the MOPA array elements feature excellent far-field properties at driving conditions for maximum single-mode power. The inset of Fig. 3 shows the lateral far-field intensity distribution for three representative devices as measured by a Mercury Cadmium Telluride detector at a distance of 9 cm from the output facet. Nine devices (2, 3, 4, 5, 7, 10, 11, 13, 15) show pure TM_{00} operation with full width at half-maximum (FWHM) angles between 5.6° and 7° (represented by the red curve in Fig. 3). One device (6, green curve in the inset of Fig. 3) features a broader angular intensity distribution with a FWHM angle of 9.4°, which is attributed to a

fabrication-induced asymmetry in the waveguide or a facet defect. Five devices (1, 8, 9, 12, 16) exhibit minor contributions of higher order lateral modes, while still maintaining an excellent far-field quality with FWHM values between 5.6° and 7.2°, represented by device 1 in Fig. 3 (blue curve). The array elements' FWHM values for the angular intensity distribution compare well to the theoretical estimate for the diffraction limited in-plane divergence angle, which was obtained by approximating the in-plane intensity distribution of the ridge mode (squared sinusoid) by a Gaussian distribution with equivalent standard deviation. For a facet width of $w = 110\,\mu$m (Gaussian spot size $w_0^g = 39.6\ \mu$m), an average FWHM of $\Theta = 5.2°$ is estimated from $\Theta = 180°/\pi \cdot \sqrt{2\ln 2} \cdot \lambda/(\pi \cdot w_0^g)$,[17] where λ is the average array wavelength.

In Fig. 4, light/amplifier-current characteristics are shown for a series of DFB currents. The curves show data for device 5 which are representative of all devices except device 3, which shows a higher rollover current than the other array elements. The curves presented in Fig. 4 exhibit typical MOPA characteristics:[14] For low DFB currents, the output power P_{out} increases exponentially with the amplifier current density j above the transparency current density j_{trans}, as given by $P_{out} = P_{in} \cdot e^{(-\alpha_w + g\cdot\Gamma\cdot(j - j_{trans}))\cdot d} = P_0 \cdot e^{g\cdot\Gamma\cdot j\cdot d}$, where P_{in} is the input power from the DFB section, α_w are the waveguide losses, d is the amplifier length, and $g \cdot \Gamma$ is the modal gain coefficient.[14] An exponential fit of the characteristics for a DFB current of 1.4 A, which does not show any signs of gain saturation, allows the extraction of the modal gain coefficient (pink dotted line in Fig. 4). A value of $g \cdot \Gamma = 4.7$ cm/kA was obtained. For DFB currents above 1.4 A, the characteristics in Fig. 4 start deviating from the exponential behavior and for a DFB current of 2.1 A show a linear dependence on amplifier currents above 4.5 A. This is an unambiguous sign of gain saturation in the amplifier and indicates that the output power can be further increased by increasing the tapering angle of the amplifier section in future devices. MOPA arrays are promising systems for studying gain saturation,[18] since they enable the separate tuning of the DFB input power and the amplifier pump current, thus, making it possible to distinguish between saturation due to high optical pumping and saturation due to band misalignments. Furthermore, a MOPA array allows saturation studies to be carried out at different points in the gain spectrum.

In conclusion, we have reported the design, fabrication, and thorough characterization of a QCL MOPA array. Each array element covers a different wavelength between 9.2 and 9.8 μm at single-mode operation, with peak powers between 0.8 and 3.9 W in pulsed operation at room temperature. In addition to the high output power, excellent far-field properties with in-plane divergence angles around 6° render the QCL MOPA array highly suitable for stand-off detection and spectroscopy applications.

The authors acknowledge the Center for Nanoscale Systems (CNS) at Harvard University. Harvard CNS is a member of the National Nanotechnology Infrastructure Network (NNIN). The authors further acknowledge Leo Missaggia for packaging the laser array. This project received support from the Defense Threat Reduction Agency-Joint Science and Technology Office for Chemical and Biological Defense (Grant no. HDTRA1-10-1-0031-DOD). P. Rauter acknowledges support from the Austrian Science Fund (FWF): J 3092-N19. The Lincoln Laboratory portion of this work was sponsored by the Office of the Assistant Secretary of Defense for Research and Engineering under Air Force Contract No. FA8721-05-C-0002. The opinions, interpretations, conclusions, and recommendations are those of the authors and are not necessarily endorsed by the United States Government.

[1]J. Faist, F. Capasso, D. L. Sivco, C. Sirtori, A. L. Hutchinson, and A. Y. Cho, Science **22**, 553 (1994).
[2]C. Gmachl, F. Capasso, D. L. Sivco, and A. Y. Cho, Rep. Prog. Phys. **64**(11), 1533 (2001).
[3]A. K. Goyal, M. Spencer, M. Kelly, J. Costa, M. DiLiberto, E. Meyer, and T. Jeys, Proc. SPIE **8018**, 80180N (2011).
[4]C. A. Kendziora, R. M. Jones, R. Furstenberg, M. Papantonakis, V. Nguyen, and R. A. McGill, Proc. SPIE **8373**, 83732H (2012).
[5]K. Degreif, S. Rademacher, P. Dasheva, F. Fuchs, S. Hugger, F. Schnürer, and W. Schweikert, Proc. SPIE **7945**, 79450P (2011).
[6]For a review on external cavity QCLs, see A. Hugi, R. Maulini, and J. Faist, Semicond. Sci. Technol. **25**, 083001 (2010).
[7]E. Mujagic, C. Schwarzer, Y. Yao, J. Chen, C. Gmachl, and G. Strasser, Appl. Phys. Lett. **98**, 141101 (2011).
[8]B. G. Lee, M. A. Belkin, C. Pflügl, L. Diehl, H. A. Zhang, R. M. Audet, J. MacArthur, D. P. Bour, S. W. Corzine, G. E. Höfler, and F. Capasso, IEEE J. Quantum Electron. **45**, 554 (2009).
[9]Q. Y. Lu, Y. Bai, N. Bandyopadhyay, S. Slivken, and M. Razeghi, Appl. Phys. Lett. **98**, 181106 (2011).
[10]H. Zhang, A. Seetharaman, P. Johnson, G. Luo, and H. Q. Le, IEEE Photon. Technol. Lett. **17**(1), 13 (2005).
[11]M. Troccoli, C. Gmachl, F. Capasso, D. L. Sivco, and A. Y. Cho, Appl. Phys. Lett. **80**(22), 4103 (2002).
[12]H. Wenzel, K. Paschke, O. Brox, F. Bugge, J. Fricke, A. Ginolas, A. Knauer, P. Ressel, and G. Erbert, Electron. Lett. **43**(3), 160 (2007).
[13]D. Mehuys, D. F. Welch, R. G. Waarts, R. Parke, A. Hardy, and W. Streifer, IEEE J. Quantum Electron. **27**(7), 1900 (1991).
[14]S. Menzel, L. Diehl, C. Pflügl, A. Goyal, C. Wang, A. Sanchez, G. Turner, and F. Capasso, Opt. Express **19**, 16229 (2011).
[15]A. Wittmann, T. Gresch, E. Gini, L. Hvozdara, N. Hoyler, M. Giovannini, and J. Faist, IEEE J. Quantum Electron. **44**, 36 (2008).
[16]K. Utaka, S. Akiba, K. Sakai, and Y. Matsushima, IEEE J. Quantum Electron. **22**, 1042 (1986).
[17]A. Yariv and P. Yeh, *Photonics: Optical Electronics in Modern Communications*, 6th ed. (Oxford University Press, 2006), Chap. 16.
[18]For the use of a two-section device for studying gain saturation, see, S. Barbieri, C. Sirtori, H. Page, M. Beck, J. Faist, and J. Nagle, IEEE J. Quantum Electron. **36**, 736 (2000).